JOURNAL OF COMPUTATIONAL PHYSICS 102, 319–335 (1992)

A Split-Matrix Runge–Kutta Type Space Marching Procedure

C. WEILAND

Messerschmitt-Bölkow-Blohm GmbH, Space Systems Group, KT32, 8000 Munich 80, Germany

Received February 24, 1990; revised April 3, 1991

A new space-marching method for the integration of the Euler equations is developed. It is robust and can deal with more complicated configurations. The Euler equations are formulated quasi-conservatively and a split-matrix method is used in order to apply a proper upwind discretisation. The eigenvalues and the eigenvectors of the rather complicated hyperbolic system in space are calculated. The bow shock is fitted using the Rankine–Hugoniot equations together with the suitable characteristic compatibility equation. The calculation of the flow variables at the wall is carried out by using a modification of the "post correction" technique which is explained in detail in this paper. The finite difference equations have been solved by applying a three-step Runge–Kutta scheme, which was also successfully used for the solution of the time-dependent Euler equations. The validation of the method is done by a careful discussion and a detailed comparison of the results with the ones of other methods. Some three-dimensional applications will be given.

1. INTRODUCTION

The development of future space transportation systems requires effective tools for the determination of hypersonic flow fields. For pure supersonic or hypersonic flow regions the application of space-marching methods is the most economical way to treat the aerodynamical problems. External flow fields around re-entry bodies like HERMES or two-stage systems to orbit like EHTV/upper stage (European hypersonic transport vehicle) contain complicated systems of strong and weak discontinuities (shocks and shear layers) which may interact with one another. Internal flow fields like inlet and nozzle flows are of the same complexity.

There exist a lot of space marching methods for the solution of the steady Euler equations, e.g., [1–8]. A time-dependent method which has the ability to step in space, if the velocity in the marching direction is supersonic, employing a modern upwind biased TVD-scheme is reported in [9]. The general strategy in modern methods is to use the characteristic wave propagation idea for constructing appropriate discrete schemes. For that one needs an eigenvalue decomposition of the corresponding flux matrices. For a set of primitive variables this can be found in [10]. For the conservative variables the decomposition is given in this paper.

A set of right-hand eigenvectors for cartesian coordinates (3D case) is proposed in [11] and a complete similarity transformation for the two-dimensional cartesian case is presented in [12].

Some of the above-mentioned methods have their undeniable merits for flow field calculations around simple and smooth bodies (see, for example, [13]), where changes of the curvature of the body contour are not too large, especially in the case of concave curvatures. Concave contours lead to the production of embedded shock waves which may or may not interact with the bow shock. In the past this often was the reason for stability problems which could not be overcome.

In this paper a robust split-matrix method for the integration of the three-dimensional steady Euler equations in general coordinates is presented. The Euler equations are formulated quasi-conservatively.

The marching operator is solved by a Runge–Kutta space-stepping procedure. In the case of external flows the bow shock can be both fitted or captured. In the bow shock fitting case this means that the numerical grid used is a function of the solution and will be generated during the computation step by step.

The algorithm for impermeable boundaries is given by the post-correction technique [14, 16] applied to the appropriate characteristic compatibility equation for steady three-dimensional Euler equations. An upwind biased third-order discretisation with respect to the characteristic direction is used to approximate the partial derivatives in the crossflow plane.

The goal for the development of this robust method was to have a numerical tool with which the flow field around rather complicated three-dimensional space transportation systems can be determined. Therefore, detailed results are presented for the above-mentioned two-stage system at two trajectory points.

0021-9991/92 $5.00

2. THE STEADY EQUATIONS OF MOTION

The unsteady quasi-conservative Euler equations have a good shock capturing capability as was demonstrated in [17], where blunt body flows were calculated with Mach numbers up to $M_\infty = 4$. The presented results compare well with the ones of a shock fitting method. The same is valid for the steady quasi-conservative Euler equations, especially because in pure supersonic or hypersonic flows the embedded shocks are only weak [6–8]. In cartesian coordinates one has

$$J\frac{\partial U}{\partial z} + K\frac{\partial U}{\partial x} + L\frac{\partial U}{\partial y} = 0. \tag{1}$$

The system (1) is hyperbolic in the z direction which means that the matrices $J^{-1}K$ and $J^{-1}L$ have only real eigenvalues. For arbitrary coordinates (ξ, η) in the crossflow plane—while the z-coordinate is retained—one obtains

$$J\frac{\partial U}{\partial z} + \bar{K}\frac{\partial U}{\partial \xi} + \bar{L}\frac{\partial U}{\partial \eta} = 0 \tag{2}$$

with $U^{\mathrm{T}} = (\rho, \rho u, \rho v, \rho w, e)$ and the total energy per unit volume is

$$e = \frac{1}{\gamma - 1}p + \frac{1}{2}\rho(u^2 + v^2 + w^2)$$

(ρ is density; p is pressure; u, v, w are cartesian velocity components).

The matrices $J, \bar{K}, \bar{L}$ can be found in the Appendix, where $\bar{K}$ and $\bar{L}$ are defined by

$$\bar{K} = J\xi_z + K\xi_x + L\xi_y,$$
$$\bar{L} = J\eta_z + K\eta_x + L\eta_y.$$

The system of Eq. (2) is to be solved by a split matrix method similar to that in [15–17] for the unsteady equations. Therefore one has to diagonalize the matrices $J^{-1}\bar{K}$ und $J^{-1}\bar{L}$. (Because the procedure is the same for both matrices, only $J^{-1}\bar{K}$ has to be considered. In the case of $J^{-1}\bar{L}$, one has to replace ξ by η.)

The eigenvalues λ are calculated using the relation

$$\det |J^{-1}\bar{K} - \lambda I| = 0, \quad I = \text{identity matrix}. \tag{3}$$

This reduces to

$$(\lambda u - \Theta_\xi)^3 [(\lambda u - \Theta_\xi)^2 - c^2(\lambda^2 - 2\xi_z\lambda + |\nabla\xi|^2)] = 0 \tag{4}$$

with $|\nabla\xi| = \sqrt{\xi_z^2 + \xi_x^2 + \xi_y^2}$

and $\Theta_\xi =$ the contravariant velocity component in the ξ-direction:

$$\Theta_\xi = u\xi_z + v\xi_x + w\xi_y.$$

One has

$$\lambda_{1/3} = \Theta_\xi/u$$
$$\lambda_{4/5} = \frac{\left(\pm\sqrt{(u^2 - c^2)(\xi_x^2 + \xi_y^2) + (v\xi_x + w\xi_y)^2}\, c\right) - c^2\xi_z + u\Theta_\xi}{u^2 - c^2} \tag{5}$$

(see also Ref. [10])

In order to diagonalize the matrix $J^{-1}\bar{K}$ using the equation

$$T_\xi^{-1}J^{-1}\bar{K} - \Lambda_{J^{-1}\bar{K}}T_\xi^{-1} = 0 \tag{6}$$

or

$$(J^{-1}\bar{K} - \lambda_j I)\, R_j^{\bar{q}} = 0 \tag{7}$$

for the right-hand eigenvector $R_j^{\bar{q}}$

$$(L_j^{\bar{q}})^{\mathrm{T}}\,(J^{-1}\bar{K} - \lambda_j I) = 0 \tag{8}$$

for the left-hand eigenvector $L_j^{\bar{q}}, j = 1 \cdots 5$,

$\bar{q}$ denotes quasi-conservative

with

$$\Lambda_{J^{-1}\bar{K}} = \begin{Bmatrix} \lambda_1 & & & & \\ & \lambda_2 & & & 0 \\ & & \lambda_3 & & \\ & & & \lambda_4 & \\ 0 & & & & \lambda_5 \end{Bmatrix},$$

one has to determine the matrices of the right-hand eigenvectors T_ξ and the left-hand eigenvectors T_ξ^{-1}.

The matrix $J^{-1}\bar{K}$ looks so complicated that it seems completely impossible to carry out the arithmetic work for the determination of the eigenvectors evaluating Eq. (6) ($J^{-1}\bar{K}$ is given in the Appendix).

One way to overcome this problem consists in considering the equations of motion in non-conservative variables, $Y^{\mathrm{T}} = (\rho, u, v, w, p)$. One has

$$A\frac{\partial Y}{\partial z} + \bar{B}\frac{\partial Y}{\partial \xi} + \bar{C}\frac{\partial Y}{\partial \eta} = 0. \tag{2a}$$

It is well known that the matrices A, $\bar{B}$, $\bar{C}$ are connected

with the matrices J, $\bar{K}$, $\bar{L}$ by a similarity transformation (see, e.g., [7]). For example, one obtains

$$\bar{B} = M^{-1}\bar{K}M. \tag{9}$$

(The matrices A, B, $\bar{B}$, M, M^{-1} can be found in the Appendix.)

This means that $A^{-1}\bar{B}$ and $J^{-1}\bar{K}$ have the same eigenvalues, Eqs. (5), and the eigenvectors are calculated by

$$(A^{-1}\bar{B} - \lambda_j I)\, R_j^{\bar{n}} = 0 \tag{7a}$$

or

$$(L_j^{\bar{n}})^{\mathrm{T}}\,(A^{-1}\bar{B} - \lambda_j I) = 0, \tag{8a}$$

where $\bar{n}$ denotes non-conservative.

Then the relations hold:

$$MR_j^{\bar{n}} = R_j^{\bar{q}}; \qquad (L_j^{\bar{n}})^{\mathrm{T}}\, M^{-1} = (L_j^{\bar{q}})^{\mathrm{T}}. \tag{10}$$

It may be of interest to know that, in the two-dimensional case, the eigenvectors are independent of the selected coordinate system. Let the frame of reference be chosen by the cartesian coordinates (x, y) and the arbitrary coordinates by (ξ, η) with $\xi(x, y)$ and $\eta(x, y)$. The total derivatives are defined by

$$\begin{aligned} d\xi &= \xi_x\, dx + \xi_y\, dy \\ d\eta &= \eta_x\, dx + \eta_y\, dy. \end{aligned} \tag{11}$$

The eigenvalue equation in (x, y) coordinates is

$$\det(B - \mu_i A) = 0 \tag{12a}$$

with

$$\mu_i \equiv \left.\frac{dy}{dx}\right|_i \quad (\triangleq \text{ direction of the Mach lines and direction of the streamline, } i = 1, 2, 3)$$

and in (ξ, η) coordinates,

$$\det(\bar{B} - \delta_i \bar{A}) = 0 \tag{12b}$$

with

$$\delta_i \equiv \left.\frac{d\eta}{d\xi}\right|_i;$$

$\bar{A} = A\xi_x + B\xi_y$, $\bar{B} = A\eta_x + B\eta_y$, A and B are the two-dimensional variants of the matrices in Eq. (2a).

Then from Eqs. (11), (12a), (12b) it follows that

$$\left.\frac{dy}{dx}\right|_i \equiv \mu_i = \frac{-\eta_x + \delta_i \xi_x}{\eta_y - \delta_i \xi_y} \tag{13}$$

and, finally, the characteristic equations

$$(B - \mu_i A)\, \bar{R}_i = 0 \tag{14a}$$

$$(\bar{B} - \delta_i \bar{A})\, \bar{\bar{R}}_i = 0 \tag{14b}$$

are valid (see Eq. (7a)). Up to a constant the right-hand eigenvectors $\bar{R}_i$ and $\bar{\bar{R}}_i$ are identical. This is not admissible in three dimensions.

The diagonalisation procedure for the matrices of the non-conservative equation of motion is, for example, given by

$$Q_\xi^{-1} A^{-1}\bar{B} - \Lambda_{A^{-1}B} Q_\xi^{-1} = 0. \tag{6a}$$

The right-hand eigenvectors $R_{1,2,3}^{\bar{n}}$ belonging to the triple eigenvalue λ_{1-3} have in common that the fifth component has to be zero. They are constructed such that neither the left-hand eigenvectors for the non-conservative equations nor the right- and left-hand eigenvectors for the quasi-conservative equations are being singular in any possible point of an appropriate flow field.

One finds

$$Q_\xi = \begin{Bmatrix} 0 & 1 & 0 & \rho(d^2 + x_1^2) & \rho(d^2 + x_1^2) \\ u & 0 & 0 & -(dx_2 + ux_1^2) & dx_2 - ux_1^2 \\ v & -\xi_y & \xi_y & \xi_x(du - x_2) & -\xi_x(du + x_2) \\ w & \xi_x & -\xi_x & \xi_y(du - x_2) & -\xi_y(du + x_2) \\ 0 & 0 & 0 & \rho(u^2 x_1^2 + x_2^2) & \rho(u^2 x_1^2 + x_2^2) \end{Bmatrix} \tag{15a}$$

$$Q_\xi^{-1} = \frac{1}{x_4} \begin{Bmatrix} 0 & ux_1^2 & x_2\xi_x \\ x_4 & 0 & 0 \\ x_4 & -u(v\xi_y - w\xi_x) & u^2\xi_y + wx_2 \\ 0 & -x_2/2d & u\xi_x/2d \\ 0 & x_2/2d & -u\xi_x/2d \end{Bmatrix}$$

$$\begin{matrix} x_2\xi_y & x_1^2/\rho \\ 0 & -(d^2 + x_1^2) \\ -(u^2\xi_x + vx_2) & -(d^2 + x_1^2) - (v\xi_y - w\xi_x)/\rho \\ u\xi_y/2d & 1/2\rho \\ -u\xi_y/2d & 1/2\rho \end{matrix} \Bigg\}. \tag{15b}$$

The abbreviations are:

$$x_1^2 = \xi_x^2 + \xi_y^2$$
$$x_2 = v\xi_x + w\xi_y$$
$$x_4 = u^2 x_1^2 + x_2^2$$
$$d^2 = \frac{x_4}{c^2} - x_1^2$$
$$q^2 = u^2 + v^2 + w^2$$
$$\delta_1 = \gamma - 1,$$

γ = ratio of specific heats,

c = the speed of sound.

And finally by the similarity transformation one obtains

$$MQ_\xi = T_\xi \qquad \text{and} \qquad Q_\xi^{-1} M^{-1} = T_\xi^{-1}.$$

The matrices T_ξ and T_ξ^{-1} are lengthy; they are written down in the Appendix (A9), (A10).

The matrices in Eq. (2) are split due to the sign of their eigenvalues. One obtains

$$\frac{\partial U}{\partial z} + (J^{-1}\bar{K})^+ \frac{\partial U}{\partial \xi}\bigg|^+ + (J^{-1}\bar{K})^- \frac{\partial U}{\partial \xi}\bigg|^- + (J^{-1}\bar{L})^+ \frac{\partial U}{\partial \eta}\bigg|^+ + (J^{-1}\bar{L})^- \frac{\partial U}{\partial \eta}\bigg|^- = 0 \tag{16}$$

with

$$(J^{-1}\bar{K}) = (J^{-1}\bar{K})^+ + (J^{-1}\bar{K})^- = T_\xi(\Lambda^+_{J^{-1}\bar{K}} + \Lambda^-_{J^{-1}\bar{K}})\, T_\xi^{-1}.$$

The space derivatives in the crossflow plane are approximated by third-order upwind-biased formulas which are already used in the time dependent split-matrix methods [17, 18]:

$$U_\xi|_m^+ = \frac{1}{6\Delta_\xi}(U_{m-2} - 6U_{m-1} + 3U_m + 2U_{m+1})$$
$$U_\xi|_m^- = -\frac{1}{6\Delta_\xi}(U_{m+2} - 6U_{m+1} + 3U_m + 2U_{m-1}). \tag{17}$$

After introducing the approximations for the space derivatives of the crossflow in Eq. (16) one has an ordinary differential equation in the hyperbolic coordinate z. This differential equation is solved using a three-step Runge–Kutta scheme, which has the form

$$\begin{aligned} U^{(0)} &= U^n \\ U^{(1)} &= U^n - a_1 \Delta z\, P(U^n) \\ U^{(2)} &= U^n - a_2 \Delta z\, P(U^{(1)}) \\ U^{(3)} &= U^n - a_3 \Delta z\, P(U^{(2)}) \\ U^{n+1} &= U^{(3)}. \end{aligned} \tag{18}$$

$P(U)$ contains the numerical approximation of the spatial derivatives in the crossflow directions $\bar{P}(U)$ and a nonlinear artificial diffusion term D which is necessary to prevent oscillations near shock waves. One has

$$P(U) = (\bar{P}(U) - D).$$

A MacCormack type diffusion term D is selected [19]. In order to investigate the accuracy of the scheme it is assumed that U is scalar,

$$\begin{aligned} U'(z) &\equiv \frac{dU}{dz} = -P(U, z), \qquad P_U \equiv \frac{dP}{dU} \\ U''(z) &= P_U P \\ U'''(z) &= -(P_{UU} P^2(U) + (P_U)^2 P(U)), \end{aligned} \tag{19}$$

where $P(U, z) \equiv P(U)$ is independent of z.

Scheme (18) yields, for $U^{n+1} \equiv U(z + \Delta z)$,

$$U(z + \Delta z) = U^n - a_3 \Delta z \times P(U^n - a_2 \Delta z\, P(U^n - a_1 \Delta z\, P(U^n))). \tag{20}$$

In the following, the index n and the argument U of P have been dropped. The Taylor expansion is

$$U(z + \Delta z) = U - \Delta z\, P + \frac{(\Delta z)^2}{2} P_U P - \frac{1}{6}(\Delta z)^3 (P_{UU} P^2 + (P_U)^2 P) + \cdots. \tag{21}$$

Using a linearized version of P with respect to U one obtains

$$P(U - a_i \Delta z\, P) = P - a_i \Delta z\, P P_U; \tag{22a}$$

in the non-linear case one obtains at least

$$P(U - a_i \Delta z\, P) = P - a_i \Delta z\, P P_U + \tfrac{1}{2}(a_i \Delta z)^2 P^2 P_{UU}, \quad i = 1, 2, 3. \tag{22b}$$

Inserting Eq. (22a) in Eq. (20) yields

$$U(z+\Delta z) = U - a_3\,\Delta z\,P + a_3 a_2(\Delta z)^2\,PP_U - a_3 a_2 a_1(\Delta z)^3\,P(P_U)^2.$$

Comparison with Eq. (21) shows that for $a_3 = 1$ and $a_2 = \frac{1}{2}$ the scheme is second-order accurate. Employing Eq. (22b) one finds

$$U(z+\Delta z) = U - a_3\,\Delta z\,P + a_3 a_2(\Delta z)^2\,PP_U - \tfrac{1}{2}a_3 a_2(\Delta z)^3(2a_1 P(P_U)^2 + \underline{a_2 P^2 P_{UU}}) + O((\Delta z)^4).$$

Also in this case only second-order accuracy can be attained ($a_3 = 1$ and $a_2 = \frac{1}{2}$). The underlined term can be regarded as the influence of the non-linear part of P on the third-order terms (see also [20]). The coefficient a_1 is chosen $a_1 \approx 0.25$. For this value the stability region can be extended to CFL = 1.75. Numerical experiments have shown that this maximum CFL number can always be applied except for flows with strong bow shock/embedded shock interactions; there the CFL number has to be reduced to CFL $\approx$ 1.35.

3. IMPERMEABLE WALL BOUNDARY CONDITION

In two dimensions the eigenvalues refer directly to the slopes of the streamline ($\lambda_{1,2}$), the right running Mach line (λ_3), and the left running Mach line (λ_4), respectively. In three dimensions the problem is more complicated, but the pictures coincide with each other if one considers the situation for a constant η-coordinate. Nevertheless, the main idea for the handling of the impermeable wall boundary condition is, that in Eq. (16) the characteristic components (the z-ξ space is considered) which transfer the influence from inside the flow field to the wall are retained ($\lambda_j \geqslant 0$; $j = 1, 2, 3, 5$), while the one component which would transfer the influence from inside the body to the wall is replaced by the kinematic boundary condition [16]. A nice formulation of this process for the unsteady Euler equations is carried out in [14]. This way will also be followed here by employing the steady Euler equations. It is assumed that the "characteristic variables" defined by $W_0^* = T_\xi^{-1} U_0^*$, calculated with the field algorithm at the wall, are correct for $j = 1, 2, 3, 5$:

$$U_0^{*\mathrm{T}} = (\rho, \rho u, \rho v, \rho w, e)_0^*$$
$$W_0^{*\mathrm{T}} = (w_1, w_2, w_3, w_4, w_5)_0^*.$$

Then by replacing the fourth component of the relation with the wall boundary condition ($\rho\Theta_\xi = 0$) one obtains

$$\begin{Bmatrix} w_1 \\ w_2 \\ w_3 \\ \rho\Theta_\xi \\ w_5 \end{Bmatrix}_0 = \begin{Bmatrix} w_1 \\ w_2 \\ w_3 \\ 0 \\ w_5 \end{Bmatrix}_0^* = (I - I_4)\,T_\xi^{-1} U_0^* \tag{23}$$

(the subscript 0 refers to $\xi = 0$ at the wall contour):

$$I = \begin{Bmatrix} 1 & & & & \\ & 1 & & & 0 \\ & & 1 & & \\ 0 & & & 1 & \\ & & & & 1 \end{Bmatrix};$$

$$I_4 = \begin{Bmatrix} 0 & & & & \\ & 0 & & & 0 \\ & & 0 & & \\ 0 & & & 1 & \\ & & & & 0 \end{Bmatrix}.$$

Let

$$\tilde{T}^{-1} = (I - I_4)\,T_\xi^{-1} + I_4 \begin{Bmatrix} 0 & 0 & 0 & 0 & 0 \\ 0 & 0 & 0 & 0 & 0 \\ 0 & 0 & 0 & 0 & 0 \\ 0 & \xi_z & \xi_x & \xi_y & 0 \\ 0 & 0 & 0 & 0 & 0 \end{Bmatrix}$$

then from Eq. (23) it follows that

$$(\tilde{T}^{-1} U_0)^{\mathrm{T}} = (w_1, w_2, w_3, \rho\Theta_\xi, w_5)_0 \tag{24}$$

and, with $I_4^2 = I_4$; $(I - I_4)\,I_4 = 0$, one finally finds

$$U_0 = \tilde{T}(I - I_4)\,\tilde{T}^{-1} U_0^* = U_0^* - \tilde{T} I_4 \tilde{T}^{-1} U_0^* = U_0^* - \Delta U_0^*. \tag{25}$$

Again the direct evaluation of the second right-hand term of Eq. (25) seems hopeless. Therefore the way via the non-conservative formulation is utilized again with

$$G = \tilde{T}^{-1}M = (I - I_4)\,Q_\xi^{-1} + I_4 \times \begin{Bmatrix} 0 & 0 & 0 & 0 & 0 \\ 0 & 0 & 0 & 0 & 0 \\ 0 & 0 & 0 & 0 & 0 \\ 0 & \xi_z & \xi_x & \xi_y & 0 \\ 0 & 0 & 0 & 0 & 0 \end{Bmatrix} M$$

$$\tilde{T} = MG^{-1}.$$

The equation for the correction of the flow variables at the wall is then

$$U_0 = U_0^* - \frac{\rho \Theta_\xi}{d[d\Theta_\xi + ux_1^2 - x_2\xi_z]} \times \begin{Bmatrix} d^2 + x_1^2 \\ d[du - x_2] \\ d^2v + du\,\xi_x + \xi_y(v\xi_y - w\xi_x) \\ d^2w + du\,\xi_y - \xi_x(v\xi_y - w\xi_x) \\ q^2\delta_1(d^2 + x_1^2) + 2(1-\delta_1)\,x_4 \end{Bmatrix}. \tag{26}$$

The calculation of the preliminary flow variables at the wall using the field algorithm requires the values in two artificial points inside the body. These points have to be determined by an extrapolation. The extrapolation formula proposed in [21] gives good results if it is applied to the points U_{-1} and U_{-2}:

$$U_k = 1.5U_{k+1} + 1.5U_{k+2} - 3.5U_{k+3} + 1.5U_{k+4}$$
$$k = -1, -2.$$

4. BOW SHOCK WAVE BOUNDARY CONDITION

The best way to deal with shock waves is to fit them. In three dimensions this will be, in general, very difficult and sometimes impossible. An exception to this rule is for bow shock waves of outer flow fields of rather arbitrary configurations. Bow shock wave fitting procedures (formulated for ideal and equilibrium real gas assumptions) for time-marching [17, 24] (time dependent grids) and space-marching [6–8] (the grid is a function of the bow shock wave contour) methods are well developed and have had their merits in the past. The method here will have the capability to fit bow shock waves, also, in the case of flows around complex configurations like hypersonic transports, re-entry vehicles, etc. The derivation of the bow shock fitting algorithm follows the philosophy in [6, 8, 17]. At the bow shock wave boundary one has six unknowns, five of them are the flow variables and one is the function of the shock contour. To determine these unknowns one has the five Rankine–Hugoniot equations and one characteristic equation carrying the information from inside the flow field along a Mach line (in a locally two-dimensional pattern) to the bow shock wave boundary.

The complete set of equations is

$$\rho V_v = \rho_\infty V_{v\infty} \quad \text{continuity} \tag{27a}$$

$$p + \rho_\infty V_{v\infty} V_v = p_\infty + \rho_\infty V_{v\infty}^2 \quad \text{normal momentum} \tag{27b}$$

$$\mathbf{V}_\tau = \mathbf{V}_{\tau\infty} \quad \text{two independent equations of the tangential momentum} \tag{27c}$$

$$\frac{e+p}{\rho} = \frac{e_\infty + p_\infty}{\rho_\infty} \quad \text{energy} \tag{27d}$$

$$I_4 T_\xi^{-1} \left\{ \frac{\partial U}{\partial z} + \lambda_4 \frac{\partial U}{\partial \xi}\bigg|^+ + A \right\} = 0 \quad \text{characteristic equation} \tag{27e}$$

with

$$\frac{e+p}{\rho} = H_0 = \frac{c^2}{\gamma - 1} + \frac{1}{2}(u^2 + v^2 + w^2),$$

H_0 = total enthalpy, e = total energy, "∞" = free stream condition

$$A = T_\eta \Lambda^+_{J^{-1}L} T_\eta^{-1} \frac{\partial U}{\partial \eta}\bigg|^+ + T_\eta \Lambda^-_{J^{-1}L} T_\eta^{-1} \frac{\partial U}{\partial \eta}\bigg|^-$$

$$V_v = \mathbf{v}\frac{\operatorname{grad}\xi}{|\operatorname{grad}\xi|}, \qquad \mathbf{V}_\tau = \mathbf{v} \times \frac{\operatorname{grad}\xi}{|\operatorname{grad}\xi|}$$

V_v = velocity component normal to the shock

$\mathbf{V}_\tau$ = velocity vector in the plane tangential to the shock.

This leads to a system of equations for the five flow variables and the function of the shock wave contour which has the form

$$\begin{Bmatrix} \rho u \\ \rho v \\ \rho w \end{Bmatrix} = \frac{\rho}{\rho_\infty} \begin{Bmatrix} \rho u \\ \rho v \\ \rho w \end{Bmatrix}_\infty + \left[1 - \frac{\rho}{\rho_\infty}\right] \frac{\alpha_\infty}{|\operatorname{grad}\xi|^2} \begin{Bmatrix} \xi_z \\ \xi_x \\ \xi_y \end{Bmatrix}$$

$$\frac{\rho}{\rho_\infty} = \frac{1}{2E}\{-F + \sqrt{F^2 - 4GE}\}$$

$$e = e_\infty \frac{\rho}{\rho_\infty} + \left(1 - \frac{\rho_\infty}{\rho}\right) \times \left(p_\infty \frac{\rho}{\rho_\infty} - \frac{\alpha_\infty^2}{|\text{grad } \xi|^2 \rho_\infty}\right)$$

$$\Phi(\xi_z) = -\frac{1}{2}\rho |\mathbf{v}|^2 + \frac{\rho}{\rho_\infty}(e_\infty + p_\infty) - \frac{\gamma}{\gamma - 1}\left[p_\infty + \frac{\alpha_\infty^2}{|\text{grad } \xi|^2 \rho_\infty} \times \left[1 - \frac{\rho_\infty}{\rho}\right]\right] = 0, \tag{28}$$

where

$$\alpha_\infty = (\rho u)_\infty \xi_z + (\rho v)_\infty \xi_x + (\rho w)_\infty \xi_y$$

$$C = \frac{\alpha_\infty}{|\text{grad } \xi|^2} t_v - t_{45} p_\infty$$

$$E = \tilde{B}_\infty - C$$

$$G = \frac{\alpha_\infty^2}{|\text{grad } \xi|^2 \rho_\infty} t_{45}$$

$$t_v = t_{42}\xi_z + t_{43}\xi_x + t_{44}\xi_y$$

$$\tilde{B}_\infty = (\rho)_\infty t_{41} + (\rho u)_\infty t_{42} + (\rho v)_\infty t_{43} + (\rho w)_\infty t_{44} + e_\infty t_{45}$$

$$\tilde{B} = \frac{\rho}{\rho_\infty}\tilde{B}_\infty + \left[1 - \frac{\rho}{\rho_\infty}\right]\frac{\alpha_\infty}{|\text{grad } \xi|^2} t_v + t_{45}\left[1 - \frac{\rho}{\rho_\infty}\right] \times \left[\frac{\rho}{\rho_\infty} p_\infty - \frac{\alpha_\infty^2}{|\text{grad } \xi|^2 \rho_\infty}\right].$$

The t_{4i} $(i = 1 \cdots 5)$ are the elements of the left-hand eigenvector matrix T_ξ^{-1} (see the Appendix).

Equation (28) is solved using a Newton iteration for ξ_z which is identical with the derivative of the shock contour function with respect to z, $F_z(z, \eta)$ for $\xi = 1$.

5. DETERMINATION OF THE SPATIAL STEP SIZE

Stability investigations of an advective type spatial scalar equation and physical considerations lead to the conditions in the z, ξ- and the z, η-space, respectively,

$$\frac{\Delta z}{\Delta \xi} \leqslant \frac{1}{\max_{m,l} |\lambda_{4,5}^\xi|}, \qquad \frac{\Delta z}{\Delta \eta} \leqslant \frac{1}{\max_{m,l} |\lambda_{4,5}^\eta|}, \tag{29}$$

where the eigenvalues $\lambda_{4,5}^k$ are calculated by Eq. (5). From this it follows for the step size Δz that

$$\Delta z \leqslant \min_{m,l} \left\{\frac{\Delta \xi}{\lambda_{4,5}^\xi}; \frac{\Delta \eta}{\lambda_{4,5}^\eta}\right\}. \tag{30}$$

Numerical experiments have shown that the relation

$$\Delta z \leqslant \text{CFL} \times \frac{(\Delta \xi \min(1/\lambda_{4,5}^\xi))(\Delta \eta \min(1/\lambda_{4,5}^\eta))}{(\Delta \xi \min(1/\lambda_{4,5}^\xi)) + (\Delta \eta \min(1/\lambda_{4,5}^\eta))} \tag{31}$$

gives best results, where CFL is defined by $\text{CFL} = (v/u)(\Delta z/\Delta x)$ (due to the advective test case). In [21] it is shown that for the corresponding time-marching three-step Runge–Kutta scheme the CFL number could be extended for the given choice of coefficients a_n (see Eq. (18)) up to $\text{CFL} = 1.75$.

6. RESULTS

To validate the new method (EULSPACE 2), comparisons are made between these results and the results found in the literature, as well as those of the centered difference scheme (EULSPACE 1), described in [6–8] (which is less robust than the new one, but gives highly accurate results).

Cone Flow

The first example is the flow around a cone with an semi-apertural angle $\varepsilon = 10°$. For the freestream Mach number $M_\infty = 2.0$, two angles of attack are considered ($\alpha = 19°$ and $25°$). Figures 1a and 2a show the isobars and the streamlines in the conical crossflow plane taken from Ref. [22]. These results are compared with the present ones in Figs. 1b and 2b. The beginning crossflow shock can

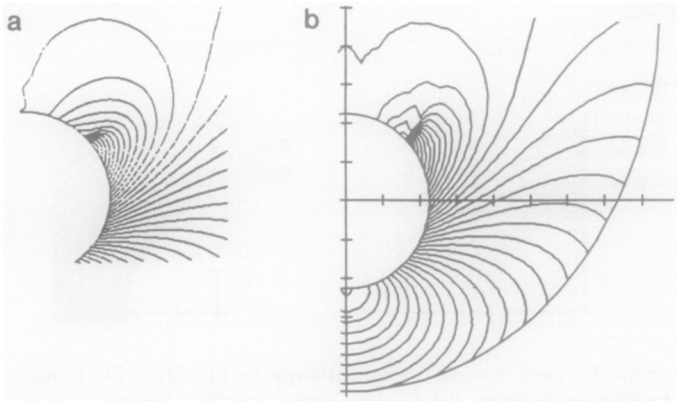

FIG. 1. Cone flow, semi-apertural angle $\varepsilon = 10°$, $M_\infty = 2.0$: (a) Isobars, $\alpha = 19°$, Ref. [22]; (b) Isobars, $\alpha = 19°$, EULSPACE 2.

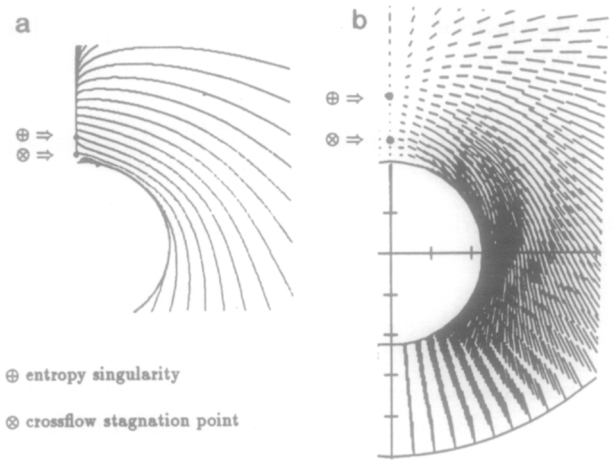

FIG. 2. Cone flow, semi-apertural angle $\varepsilon = 10°$, $M_\infty = 2.0$: (a) Streamlines in conical crossflow plane, entropy singularity, and crossflow stagnation point, $\alpha = 19°$, Ref. [22]; (b) Conical crossflow velocity vectors, entropy singularity, and crossflow stagnation point, $\alpha = 19°$, EULSPACE 2.

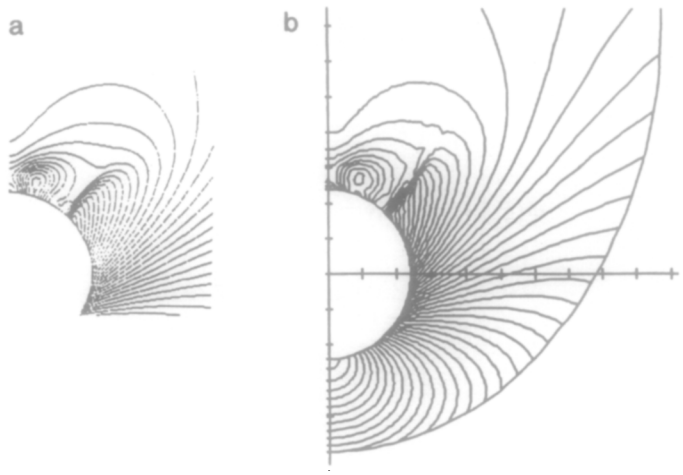

FIG. 4. Cone flow, semi-apertural angle $\varepsilon = 10°$; $M_\infty = 2.0$: (a) Isobars, $\alpha = 25°$, Ref. [22]; (b) Isobars, $\alpha = 25°$, EULSPACE 2, fitted bow shock.

clearly be seen, where in the present computation the shock was more pointed. The entropy singularity and the additional stagnation point (which is due to the formation of the spiral; for details see Ref. [22]) can be seen in Figs. 2a and 2b. However, the location of these points is different in the two compared predictions. From the tendency, the locations found in Ref. [23], Fig. 3, agree better with the ones in Fig. 2b. The computational grid has (33, 37) points in the crossflow plane ($\alpha = 19°$).

Increasing the angle of attack leads to a rise in vorticity generated at the crossflow shock, so that the spiral is now well developed. In Figs. 4a, b the pressure fields from Ref. [22] and the present one are compared. The agreement seems to be rather good.

The form and the location of the spiral displayed in Ref. [22] by streamlines (Fig. 5a) and in this solution by conical crossflow velocity vectors (Fig. 5b) look very similar. For the $\alpha = 25°$ case a grid with (33, 73) points was used.

FIG. 3. Cone flow, semi-apertural angle $\varepsilon = 10°$; $M_\infty = 2.0$: Conical crossflow streamlines, Ref. [23] ⇔ Conical crossflow velocity vectors, EULSPACE 2; entropy singularity and crossflow stagnation point, $\alpha = 20°$.

The same cone with a hypersonic freestream Mach number ($M_\infty = 8$) and an angle of attack $\alpha = 12°$ is considered in the following. Figures 6a, 7a, 8a show the solutions of EULSPACE 1 and Figs. 6b, 7b, 8b show the corresponding solutions of EULSPACE 2 (present method). In both computations the grid size was (17, 19) points in the (ξ, η) crossflow plane ($z = \text{const}$ plane).

The comparison of the Mach number isoline plot (Figs. 6a, b) shows good agreement except in a small region on the leeward side. This is due to the coarse mesh (17 points from body to shock, 19 points in the meridional half

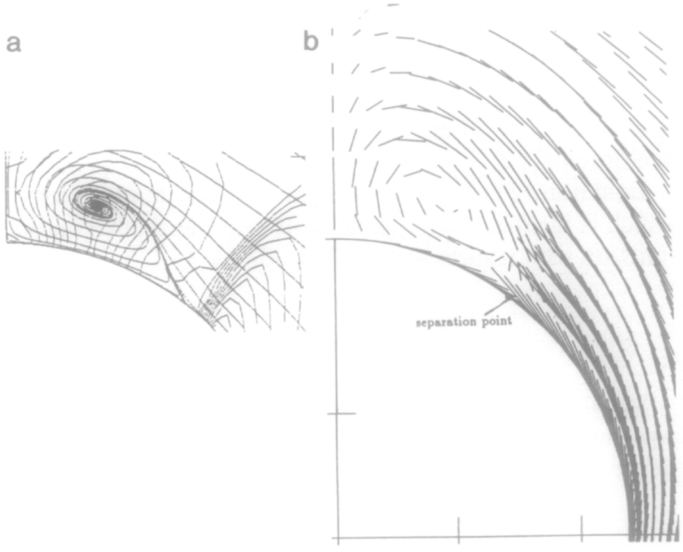

FIG. 5. Cone flow, semi-apertural angle $\varepsilon = 10°$; $M_\infty = 2.0$: (a) Conical crossflow streamlines, $\alpha = 25°$, Ref. [22]; (b) Conical crossflow streamlines, $\alpha = 25°$, EULSPACE 2.

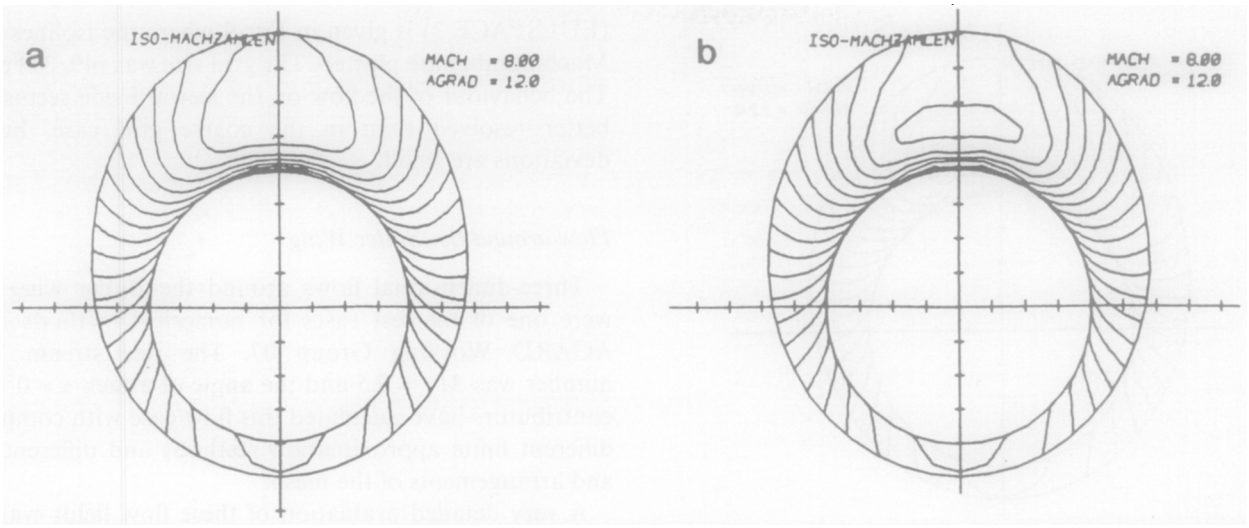

FIG. 6. Cone flow, semi-apertural angle $\varepsilon = 10°$, $M_\infty = 8$, $\alpha = 12°$, (17, 19) grid points: (a) Machnumber isolines, EULSPACE 1; (b) Machnumber isolines, EULSPACE 2.

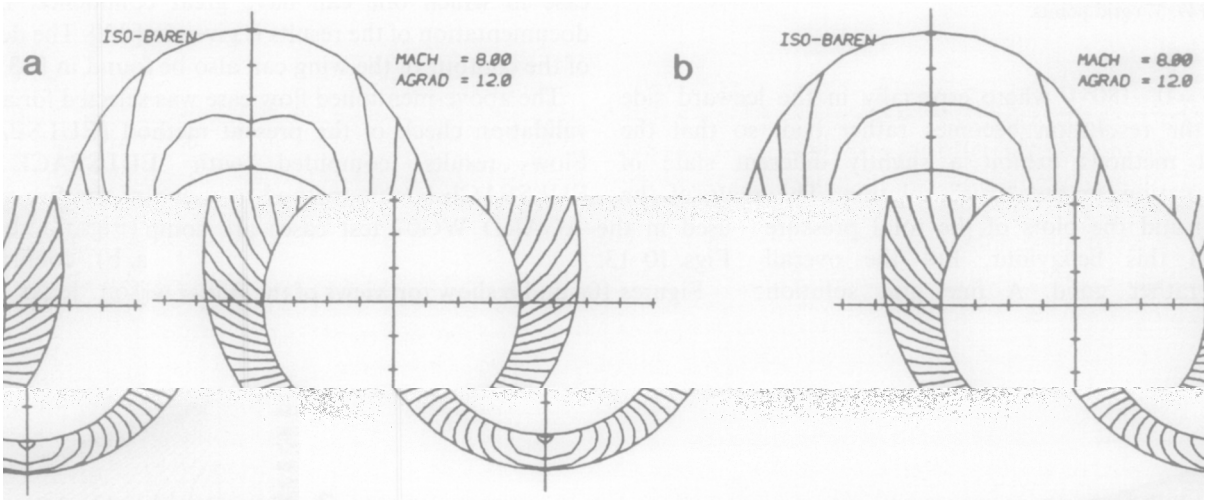

FIG. 7. Cone flow, semi-apertural angle $\varepsilon = 10°$, $M_\infty = 8$, $\alpha = 12°$, (17, 19) grid points: (a) Isobars, EULSPACE 1; (b) Isobars, EULSPACE 2.

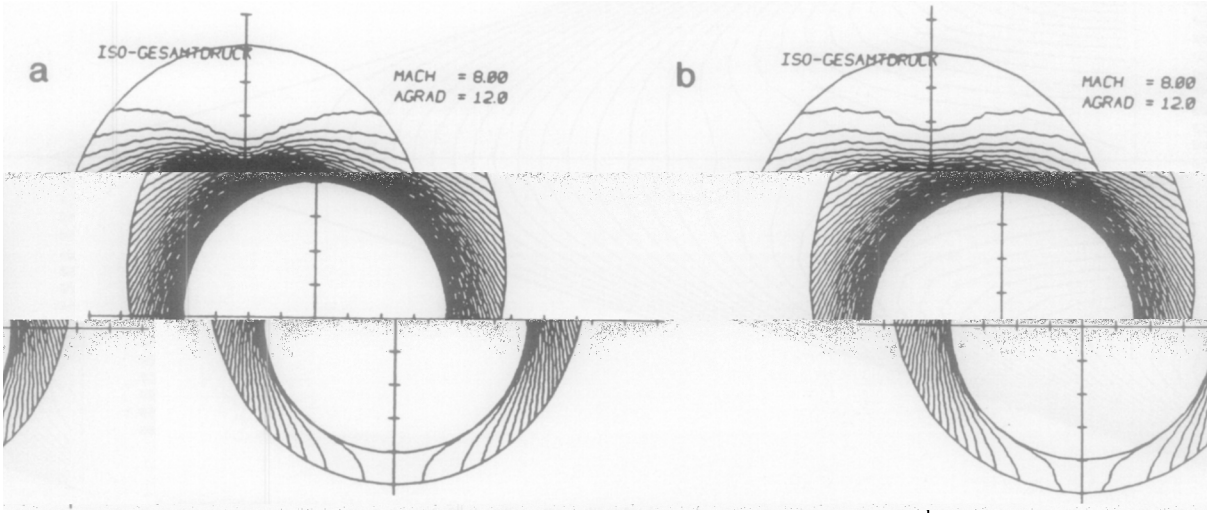

FIG. 8. Cone flow, semi-apertural angle $\varepsilon = 10°$, $M_\infty = 8$, $\alpha = 12°$, (17, 19) grid points: (a) Total pressure isolines, EULSPACE 1; (b) Total pressure isolines, EULSPACE 2.

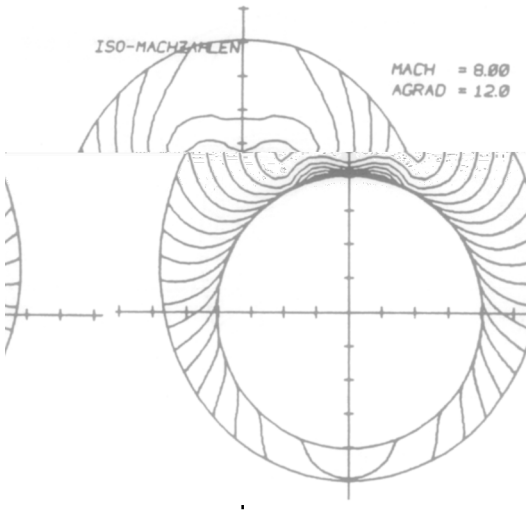

FIG. 9. Cone flow, semi-apertural angle $\varepsilon = 10°$, $M_\infty = 8$, $\alpha = 12°$, (17, 19) grid points, Machnumber isolines EULSPACE 2; fine grid solution, (49, 37) grid points.

space $\eta = 0°$–$180°$), where especially in the leeward side region the resolution becomes rather bad, so that the different methods exhibit a slightly different state of approximation to the "true" solution. The plots of the isobars (Figs. 7a, b) and the plots of the total pressure (Figs. 8a, b) confirm this behaviour. But the overall comparison looks rather good. A fine grid solution (EULSPACE 2) is given in Fig. 9 where the isolines of the Mach number are plotted. The grid size was (49, 37) points. The behaviour of the flow on the leeward side seems to be better resolved than in the coarse grid case, but the deviations are small.

Flow around the Butler Wing

Three-dimensional flows around the Butler wing [25] were one of the test cases for numerical methods in the AGARD Working Group 07. The free stream Mach number was $M_\infty = 2.5$ and the angle of attack $\alpha = 0°$. Five contributors have calculated this flow case with completely different finite approximation methods and different sizes and arrangements of the mesh.

A very detailed evaluation of these flow fields was performed and many comparisons between the five solutions were carried out. This has led to a data base for this flow case in which one can have great confidence. Detailed documentation of the results is given in [13]. The definition of the contour of the wing can also be found in [13].

The above-mentioned flow case was selected for a further validation check of the present method (EULSPACE 2). Flow results computed with EULSPACE 2 and EULSPACE 1 (this method was one of the five methods used in the AGARD WG07 test case) are compared in Figs. 10–13.

Figures 10a and b show top views of the Butler wing with

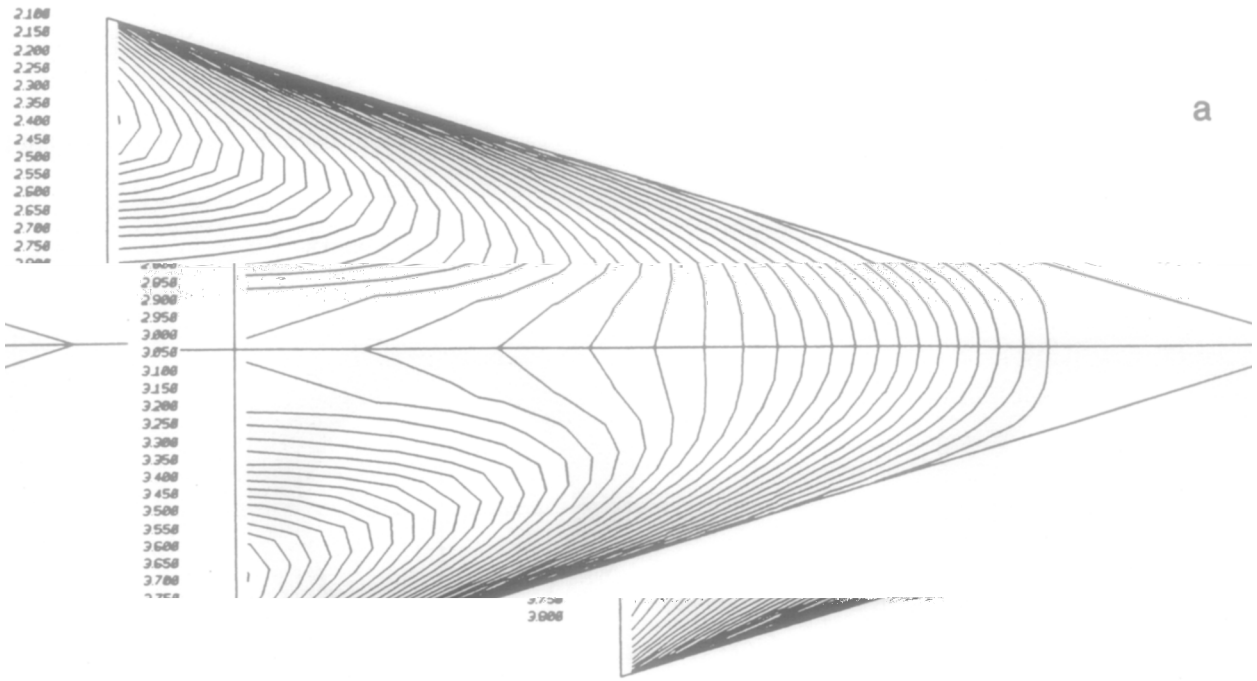

FIG. 10. Butler wing, $M_\infty = 2.5$, $\alpha = 0°$, (17, 37) grid points in crossflow planes: (a) Machnumber isolines on body surface, EULSPACE 2, increment $\Delta M = 0.05$; (b) Machnumber isolines on body surface, EULSPACE 1, increment $\Delta M = 0.05$; fine grid solution: (33, 73) grid points.

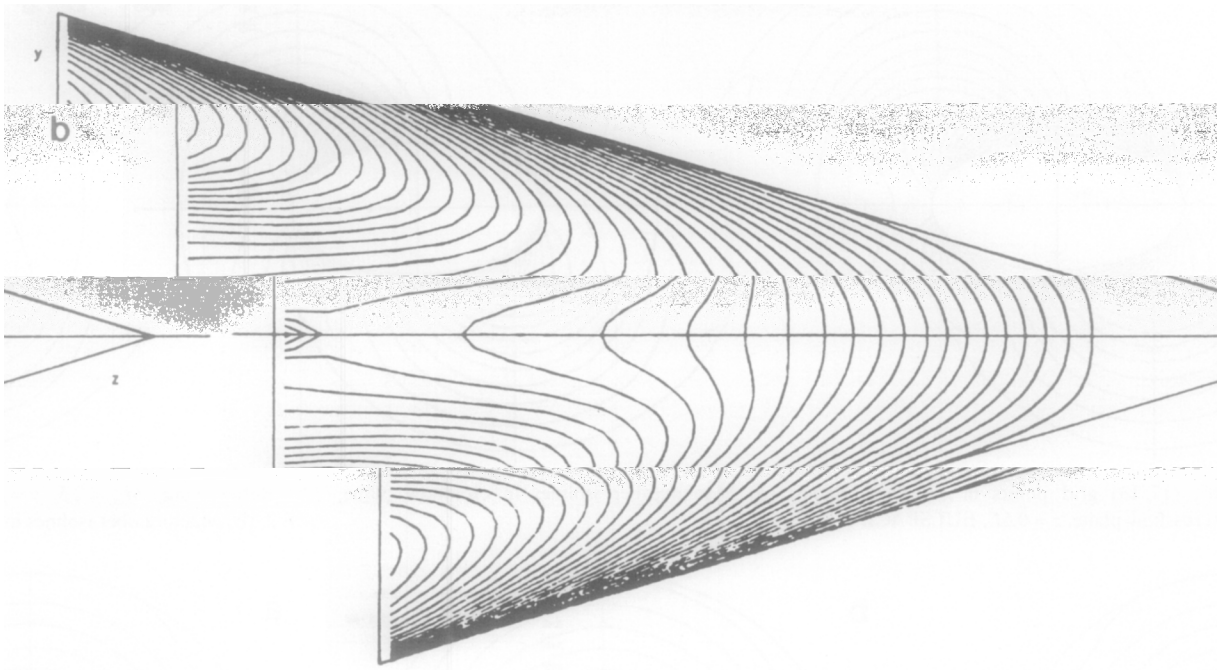

FIG. 10—*Continued*

isolines of the Mach number. Despite the fact that the solution with EULSPACE 1 [13] (Fig. 10b) was performed on a rather fine grid with (33, 73) points in the crossflow plane compared to the EULSPACE 2 (present method) solution (Fig. 10a) with a mesh of (17, 37) points, the agreement of the results is very satisfactory, with the exception of a small region in the symmetry plane in the aft part of the wing. These deviations are surely due to the coarseness of the grid in the plane of symmetry (see Fig. 11a). Figures 11–13 give the results of an EULSPACE 2 solution (Figs. 11a, 12a, 13a) and of an EULSPACE 1 solution (Figs. 11b, 12b, 13b) each on a mesh with (17, 37) points. An idea of the different mesh arrangements can be found in Figs. 11a, b in a crossflow plane $z = 0.9L$. The outer boundary of the mesh states the fitted bow shock. The plots of the Mach number isolines drawn for the two crossflow planes $z = 0.6L$ and $z = 0.95L$ (Figs. 12a, b; 13a, b) show the excellent agreement with each other.

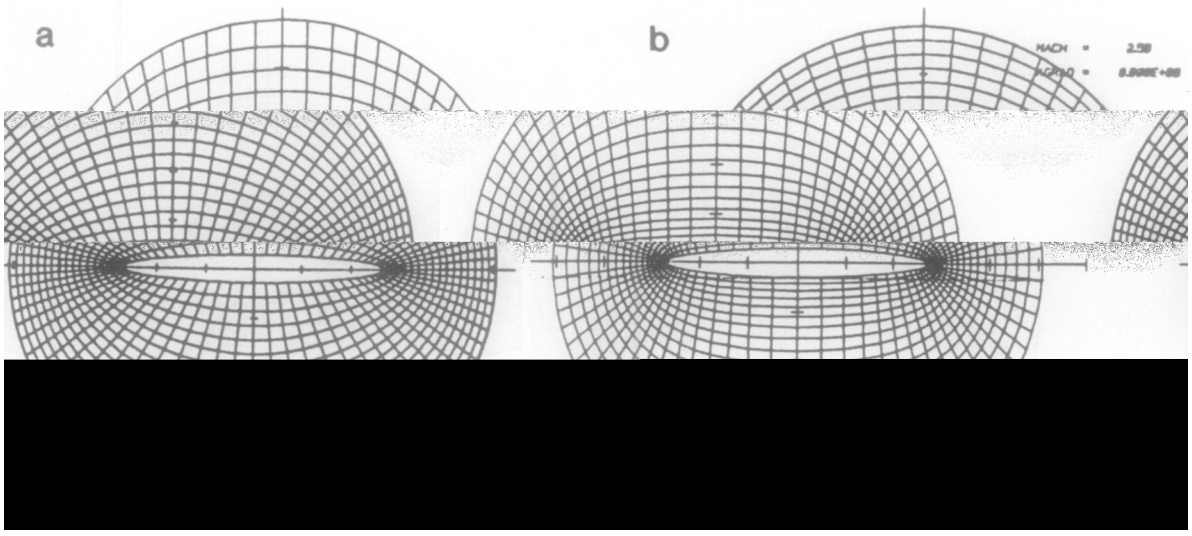

FIG. 11. Butler wind, $M_\infty = 2.5$, $\alpha = 0°$, (17, 13) grid points in crossflow planes: (a) Distribution of grid points in crossflow plane, EULSPACE 2; (b) Distribution of grid points in crossflow plane, EULSPACE 1.

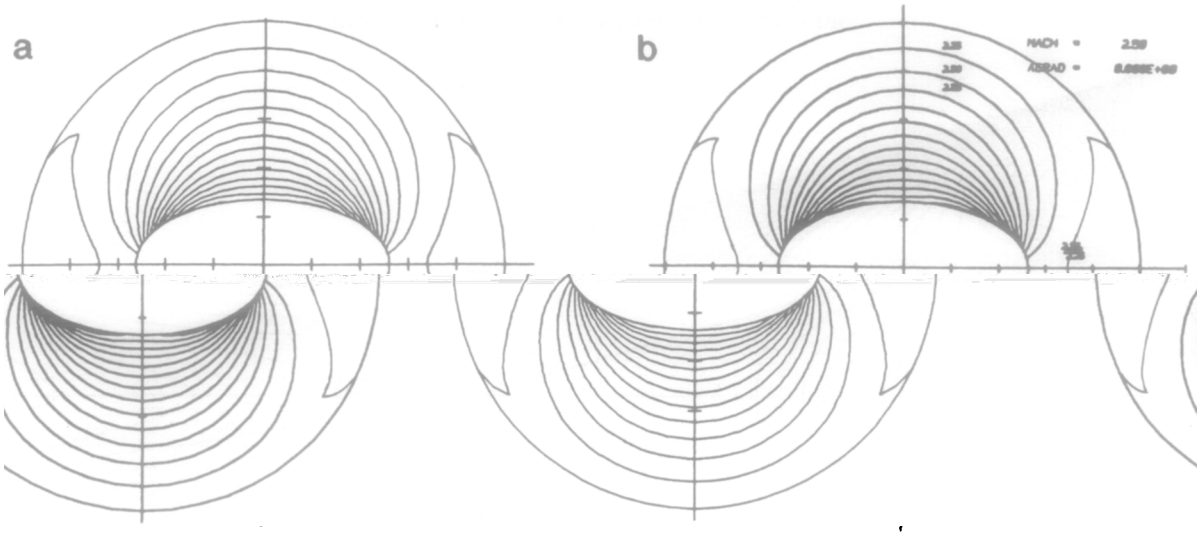

FIG. 12. Butler wing, $M_\infty = 2.5$, $\alpha = 0°$, (17, 13) grid points in crossflow planes: (a) Machnumber isolines in crossflow plane, $z = 0.6L$, EULSPACE 2; (b) Machnumber isolines in crossflow plane, $z = 0.6L$, EULSPACE 1.

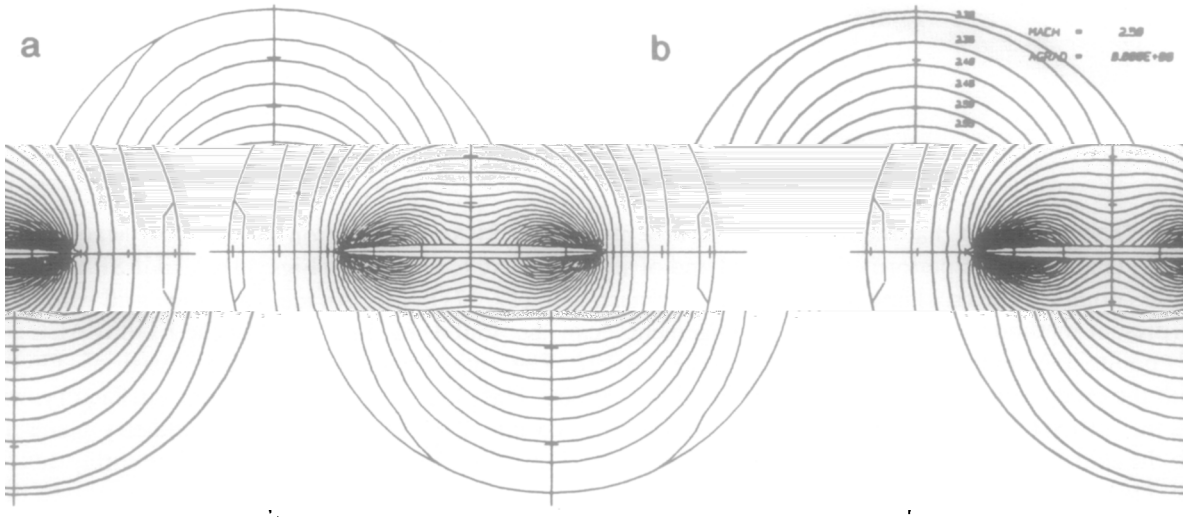

FIG. 13. Butler wing, $M_\infty = 2.5$, $\alpha = 0°$, (17, 13) grid points in crossflow planes: (a) Machnumber isolines in crossflow plane, $z = 0.95L$, EULSPACE 2; (b) Machnumber isolines in crossflow plane, $z = 0.95L$, EULSPACE 1.

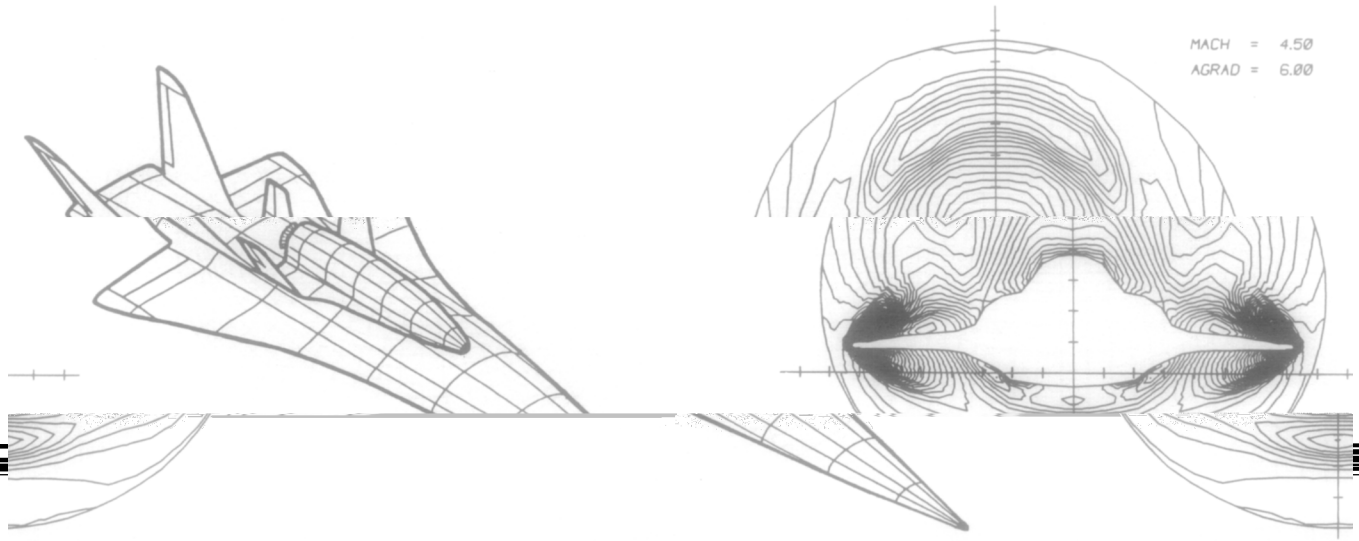

FIG. 14. Two-stage hypersonic space transportation system (EHTV) configuration.

FIG. 15. Two-stage EHTV. Isobars in crossflow plane $z = 70$m, $M_\infty = 4.5$, $\alpha = 6°$, (17, 73) grid points.

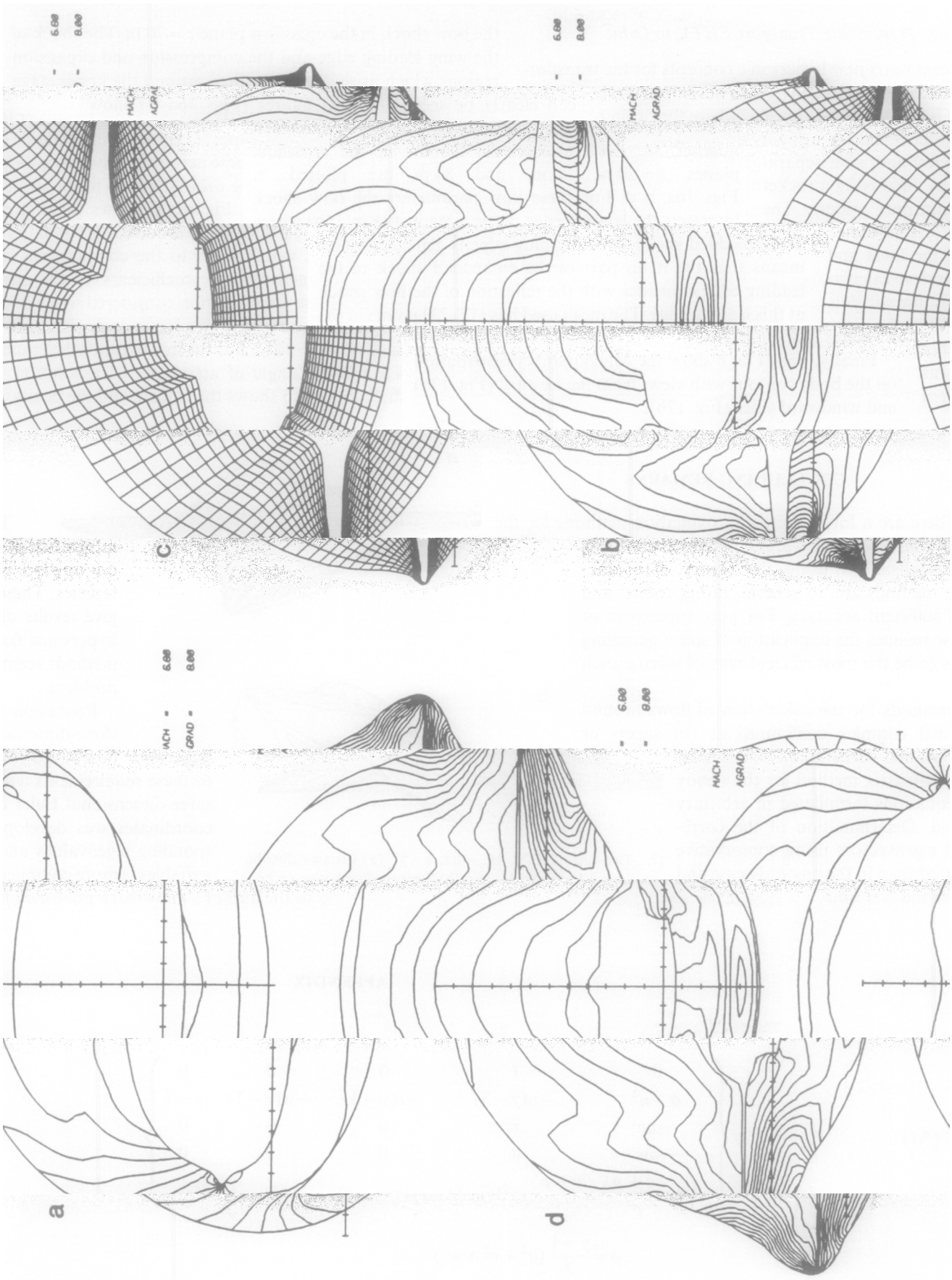

FIG. 16. Two-stage EHTV, $M_\infty = 6.8$, $\alpha = 8°$, (17, 73) grid points: (a) Isobars in crossflow plane $z = 20$m; (b) Isobars in crossflow plane $z = 70$m; (c) Distribution of grid points in crossflow plane $z = 70$m; (d) Isobars in crossflow plane $z = 84$m.

Two-Stage Hypersonic Transport EHTV to Orbit

In recent years new hypersonic concepts for the transportation of space vehicles into orbit have been developed. One of these concepts is the two-stage concept, where the orbiter is transported up to an altitude of order 35 km by using a hypersonic aerodynamic-assisted aircraft and, after separation, the orbiter travels to the orbit by employing a rocket motor. Figure 14 shows such a transport system. The prediction of the flow around this configuration is of major interest with respect to the computation of the local and global aerodynamic coefficients. In the numerical calculations the configuration considered was without the winglets of the upper and the lower stage. The total length of the lower stage was $L = 84$ m. For the free stream Mach number $M_\infty = 4.5$ and the angle of attack $\alpha = 6°$ a solution was established. Figure 15 shows the isobars and the position of the bow shock in the crossflow plane $z = 70$ m. The shock of the wing leading edge and the compression and expansion regions which arise due to the flow around the upper stage can clearly be seen. The next figures (Figs. 16a–d) show some evaluations of the flow field for the free stream Mach number $M_\infty = 6.8$ and $\alpha = 8°$. Isobars in the crossflow planes $z = 20$ m, 70 m, and 84 m are plotted in Figs. 16a, b, d. For these flow parameters the bow shock intersects the leading edge of the wing just (Fig. 16b) where the embedded shock of the leading edge is generated. This means that the main part of the embedded shock of the leading edge coincides with the reflection of the bow shock at this leading edge. The mesh used has (17, 73) points in the crossflow plane (Fig. 16c).

Finally, Figs. 17a, b show the Mach number distribution on the body contour with views from the leeward (Fig. 17a) and windward sides (Fig. 17b).

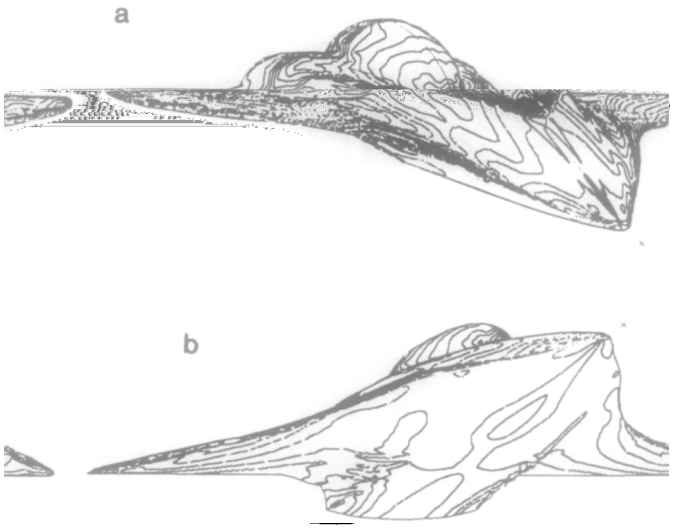

FIG. 17. Two-stage EHTV, $M_\infty = 6.8$, $\alpha = 8°$: (a) Pressure distribution on body surface leeward side view; (b) Pressure distribution on body surface windward side view.

CONCLUDING REMARKS

There are a lot of finite approximation methods for the integration of the unsteady Euler equations which are based on upwind discretisations using the theory of characteristics. These methods are, in general, rather robust and give results of sufficient accuracy. For pure supersonic or hypersonic flow regimes the application of space marching methods seems to be the most efficient way of solving such problems.

Prediction methods for the calculation of flows around three-dimensional complex configurations (in super- or hypersonic flow) need robust and efficient algorithms. Due to these requirements a split-matrix method for the steady three-dimensional Euler equations formulated in arbitrary coordinates was developed. Determination of the corresponding eigenvalues and eigenvectors using conservative variables is more complicated than in the unsteady case and is to the author's knowledge published for the first time.

APPENDIX

The matrix J:

$$J = \begin{Bmatrix} 0 & 1 & 0 & 0 & 0 \\ \phi - u^2 & -u(\gamma-3) & -v(\gamma-1) & -w(\gamma-1) & \gamma-1 \\ -uv & v & u & 0 & 0 \\ -uw & w & 0 & u & 0 \\ u\left(\phi - \dfrac{e+p}{\rho}\right) & \dfrac{e+p}{\rho} - u^2(\gamma-1) & -uv(\gamma-1) & -uw(\gamma-1) & u\gamma \end{Bmatrix}, \tag{A1}$$

$$\phi = \frac{\gamma-1}{2}(u^2+v^2+w^2).$$

The matrix $\bar{K}$:

$$\bar{K}=\begin{Bmatrix} 0 & \xi_z & \xi_x & \xi_y & 0 \\ \xi_z\phi-u\Theta_\xi & \xi_z(2-\gamma)u+\Theta_\xi & \xi_x u-\xi_z(\gamma-1)v & \xi_y u-\xi_z(\gamma-1)w & \xi_z(\gamma-1) \\ \xi_x\phi-v\Theta_\xi & \xi_z v-\xi_x(\gamma-1)u & \xi_x(2-\gamma)v+\Theta_\xi & \xi_y v-\xi_x(\gamma-1)w & \xi_x(\gamma-1) \\ \xi_y\phi-w\Theta_\xi & \xi_z w-\xi_y(\gamma-1)u & \xi_x w-\xi_y(\gamma-1)v & \xi_y(2-\gamma)w+\Theta_\xi & \xi_y(\gamma-1) \\ \left(\phi-\dfrac{e+p}{\rho}\right)\Theta_\xi & \xi_z\left(\dfrac{e+p}{\rho}\right)-(\gamma-1)\,u\Theta_\xi & \xi_z\left(\dfrac{e+p}{\rho}\right)-(\gamma-1)\,v\Theta_\xi & \xi_y\left(\dfrac{e+p}{\rho}\right)-(\gamma-1)\,w\Theta_\xi & \Theta_\xi\gamma \end{Bmatrix},$$

$$\Theta_\xi=\xi_z u+\xi_x v+\xi_y w. \tag{A2}$$

The matrix $\bar{L}$ can be obtained by replacing ξ by η in the definition of $\bar{K}$.

The matrix $J^{-1}\bar{K}$:

$$J^{-1}\bar{K}=\frac{1}{u(c^2-u^2)}\begin{Bmatrix} (c^2-u^2)\,\Theta_\xi-x_2\phi & ux_2(\delta_1+1) & -x_3 & -x_5 & -x_2\delta_1 \\ 0 & \xi_z & \xi_x & \xi_y & 0 \\ \phi[(c^2-u^2)\,\xi_x-vx_2] & -u[(c^2-u^2)\,\delta_1\xi_x-vx_2(\delta_1+1)] & -vx_3+(c^2-u^2)(\Theta_\xi-v\delta_1\xi_x) & -[vx_5+(c^2-u^2)\,w\delta_1\xi_x] & \delta_1[(c^2-u^2)\,\xi_x-vx_2] \\ \phi[(c^2-u^2)\,\xi_y-wx_2] & -u[(c^2-u^2)\,\delta_1\xi_y-wx_2(\delta_1+1)] & -[wx_3+(c^2-u^2)\,v\delta_1\xi_y] & -wx_5+(c^2-u^2)(\Theta_\xi-w\delta_1\xi_y) & \delta_1[(c^2-u^2)\,\xi_y-wx_2] \\ x_2\phi(c^2-H) & -ux_2(\delta_1+1)(c^2-H) & x_3(c^2-H) & x_5(c^2-H) & (c^2-u^2)\,\Theta_\xi+x_2\delta_1(c^2-H) \end{Bmatrix}, \tag{A3}$$

where the total enthalpy is defined by $H=(c^2-\phi)/\delta_1+q^2=(e+p)/\rho$ and $\delta_1=\gamma-1$; $x_2=v\xi_x+w\xi_y$; $x_3=u^2\xi_x-vx_2\delta_1$; $x_5=u^2\xi_y-wx_2\delta_1$; c is the speed of sound; γ denoted the ratio of specific heats; $q^2=u^2+v^2+w^2$.

The matrix A:

$$A=\begin{Bmatrix} u & \rho & 0 & 0 & 0 \\ 0 & u & 0 & 0 & 1/\rho \\ 0 & 0 & u & 0 & 0 \\ 0 & 0 & 0 & u & 0 \\ 0 & \rho c^2 & 0 & 0 & u \end{Bmatrix}. \tag{A4}$$

The matrix B:

$$B=\begin{Bmatrix} v & 0 & \rho & 0 & 0 \\ 0 & v & 0 & 0 & 0 \\ 0 & 0 & v & 0 & 1/\rho \\ 0 & 0 & 0 & v & 0 \\ 0 & 0 & \rho c^2 & 0 & v \end{Bmatrix}. \tag{A5}$$

The matrix $\bar{B}$:

$$\bar{B}=\begin{Bmatrix} \Theta_\xi & \rho\xi_z & \rho\xi_x & \rho\xi_y & 0 \\ 0 & \Theta_\xi & 0 & 0 & 1/\rho\xi_z \\ 0 & 0 & \Theta_\xi & 0 & 1/\rho\xi_x \\ 0 & 0 & 0 & \Theta_\xi & 1/\rho\xi_y \\ 0 & \rho c^2\xi_z & \rho c^2\xi_x & \rho c^2\xi_y & \Theta_\xi \end{Bmatrix}. \tag{A6}$$

The matrix $\bar{C}$ can be obtained by replacing ξ by η.

The matrix M:

$$M=\begin{Bmatrix} 1 & 0 & 0 & 0 & 0 \\ u & \rho & 0 & 0 & 0 \\ v & 0 & \rho & 0 & 0 \\ w & 0 & 0 & \rho & 0 \\ \frac{q^2}{2} & \rho u & \rho v & \rho w & \frac{1}{\delta_1} \end{Bmatrix}. \tag{A7}$$

and

$$M^{-1}=\begin{Bmatrix} 1 & 0 & 0 & 0 & 0 \\ -\frac{u}{\rho} & \frac{1}{\rho} & 0 & 0 & 0 \\ -\frac{v}{\rho} & 0 & \frac{1}{\rho} & 0 & 0 \\ -\frac{w}{\rho} & 0 & 0 & \frac{1}{\rho} & 0 \\ \frac{\delta_1}{2}q^2 & -\delta_1 u & \delta_1 v & \delta_1 w & \delta_1 \end{Bmatrix}. \tag{A8}$$

$$T_\xi=\begin{Bmatrix} 0 & 1 & 0 & \rho(d^2+x_1^2) & \rho(d^2+x_1^2) \\ \rho u & u & 0 & d\rho(du-x_2) & d\rho(du+x_2) \\ \rho v & v-\rho\xi_y & \rho\xi_y & \rho[d^2v+du\,\xi_x+\xi_y(v\xi_y-w\xi_x)] & \rho[d^2v-du\,\xi_x+\xi_y(v\xi_y-w\xi_x)] \\ \rho w & w+\rho\xi_x & -\rho\xi_x & \rho[d^2w+du\,\xi_y-\xi_x(v\xi_y-w\xi_x)] & \rho[d^2w-du\,\xi_y-\xi_x(v\xi_y-w\xi_x)] \\ \rho q^2 & \frac{q^2-2\rho(v\xi_y-w\xi_x)}{2} & \rho(v\xi_y-w\xi_x) & \frac{\rho[q^2\delta_1(d^2+x_1^2)+2(1-\delta_1)x_4]}{2\delta_1} & \frac{\rho[q^2\delta_1(d^2+x_1^2)+2(1-\delta_1)x_4]}{2\delta_1} \end{Bmatrix}; \tag{A9}$$

$$T_\xi^{-1}=\frac{1}{2\rho x_4}\begin{Bmatrix} q^2x_1^2\delta_1-2x_4 & -2ux_1^2(\delta_1-1) & -2(vx_1^2\delta_1-x_2\xi_x) & -2(wx_1^2\delta_1-x_2\xi_y) & 2x_1^2\delta_1 \\ -\rho[q^2\delta_1(d^2+x_1^2)-2x_4] & 2up\delta_1(d^2+x_1^2) & 2\rho v\delta_1(d^2+x_1^2) & 2\rho w\delta_1(d^2+x_1^2) & -2\rho\delta_1(d^2+x_1^2) \\ 2\rho x_4-q^2\delta_1[\rho(d^2+x_1^2)+v\xi_y-w\xi_x] & 2u[\rho\delta_1(d^2+x_1^2)+(\delta_1-1)(v\xi_y-w\xi_x)] & 2[\rho v\delta_1(d^2+x_1^2)+q^2\xi_y+v(\delta_1-1)(v\xi_y-w\xi_x)] & 2[\rho w\delta_1(d^2+x_1^2)-q^2\xi_x+w(\delta_1-1)(v\xi_y-w\xi_x)] & -2[\rho(d^2+x_1^2)+v\xi_y-w\xi_x] \\ \delta_1q^2/2 & -(du\,\delta_1+x_2) & -(dv\,\delta_1-u\xi_x) & -dw\,\delta_1-u\xi_y) & \delta_1 \\ \delta_1q^2/2 & -(du\,\delta_1-x_2) & -(dv\,\delta_1+u\xi_x) & -(dw\,\delta_1+u\xi_y) & \delta_1 \end{Bmatrix}. \tag{A10}$$

The abbreviations are defined in Section 2 (Eqs. (15a), (15b)).

REFERENCES

1. F. Marconi and F. Koch, NASA CR-3106, 1979 (unpublished).
2. P. Kutler, W. A. Reinhardt, and R. F. Warming, *AIAA J.* **11** (5), 657 (1973).
3. A. Rizzi and H. Bailey, in *Proceedings, 5th International Conference on Numerical Methods in Fluid Dynamics*, Lecture Notes in Physics, Vol. 59 (Springer-Verlag, Berlin, 1976), p. 347.
5. A. B. Wardlaw, J. M. Solomon, and F. P. Baltakis, *AIAA J.* **19** (7), 899 (1981).
6. C. Weiland, *J. Comput. Phys.* **29**, 173 (1978).
7. C. Weiland, in *Proceedings, AGARD-Conference, Aerodynamics of Vortical Type Flows in Three Dimensions, Rotterdam, Netherlands, 1983*, AGARD-CP-342, paper 19 (unpublished).
8. C. Weiland, M. Pfitzner, and G. Hartmann, in *Proceedings, 7th*

1987 (unpublished).

1988), p. 426.

9. K. Y. Szema, S. R. Chakravarthy, W. T. Riba, J. Byerly, and H. S. Dresser, AIAA Paper 87-0592, 1987 (unpublished).
10. S. R. Chakravarthy, Thesis, Iowa State University, Ames, 1979 (unpublished).
11. P. L. Roe, *J. Comput. Phys.* **43**, 357 (1981).
12. H. M. Glaz and A. B. Wardlaw, *J. Comput. Phys.* **58**, 157 (1985).
13. AGARD Advisory Report, No. 211, 1985 (unpublished).
14. M. Pfitzner, MBB-UK Report 0131/90 PUB = OTN-033083, 1990 (unpublished).
15. S. R. Chakravarthy, S. R. Anderson, and M. D. Salas, AIAA Paper 80-0268, 1980 (unpublished).
16. C. Weiland, in *Proceedings, 6th GAMM-Conference on Numerical Methods in Fluid Mechanics*, Notes on Numerical Fluid Mechanics, Vol. 13 (Vieweg Verlag, Wiesbaden, 1986), p. 383.
17. M. Pfitzner and C. Weiland, in *Proceedings, AGARD-Conference, Aerodynamics of Hypersonic Lifting Vehicles, Bristol, UK, 1987*, AGARD-CP-428, paper 22 (unpublished).
18. C. Weiland and M. Pfitzner, in *Proceedings, 10th International Conference on Numerical Methods in Fluid Dynamics*, Lecture Notes in Physics, Vol. 264 (Springer-Verlag, Berlin, 1986), p. 654.
19. T. H. Pulliam, AIAA Paper 85-0438, 1985 (unpublished).
20. M. Pfitzner, in *Proceedings, 2nd International Conference on Nonlinear Hyperbolic Problems*, Notes on Numerical Fluid Mechanics, Vol. 24 (Vieweg Verlag, Wiesbaden, 1988), p. 489.
21. Ch. Pöppe, HERMES Research Report Contract RDMFE 13/87, 1988 (unpublished).
22. N. Botta and M. Pandolfi, *AIAA J.* **27** (3), 293 (1989).
23. F. Marconi, *AIAA J.* **22**, 1048 (1984).
24. C. Weiland, *ZfW* **24**, 237 (1976).
25. D. S. Butler, *Proc. R. Soc.* **255**, 232 (1960).